Asian Journal of Chemistry; Vol. 32, No. 12 (2020), 3047-3056

ASIAN JOURNAL OF CHEMISTRY

https://doi.org/10.14233/ajchem.2020.22893

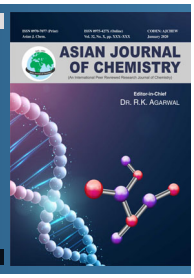

Preparation of Polyaniline/Graphene Oxide Thin Films Microelectrodes through Electrochemical Reduction at Different Potential Range for High-Performance Supercapacitors

MUKTA DAS and ASHIS K. SARKER*

Department of Chemistry, Mawlana Bhashani Science and Technology University, Santosh, Tangail-1902, Bangladesh

*Corresponding author: E-mail: ashischemru@gmail.com

Received: 9 July 2020; *Accepted*: 10 September 2020; *Published online*: 7 December 2020; AJC-20138

In this article, the fabrication and performance of supercapacitors prepared through electrochemical reduction applied at different voltage range from polyaniline/graphene oxide (PANi/GO) thin films, which are renewable materials with an excellent yield of energy conversion is reported. The PANi/GO thin film was reduced electrochemically with different potential windows, scan rate and number of cycles which was acquired using layer-by-layer (LBL) assembly method. The resultant electrodes displayed various specific capacitances after pre-reduction with different conditions.The influence of the electrochemical reduction was investigated by Raman spectroscopy and X-ray photoelectron spectroscopy for capacitance performance. The optimum conditions were explored for supercapacitor application and an elevated specific capacitance 2619 F cm^{-3} (areal capacitance 18.38 mF cm^{-2}) at 1 mV s^{-1} obtaining the film reduced with applied potential of -0.87 to -0.5 V. This study could introduce the new possibilities for the improvement of the electrochemical reduction effects to the composite materials for high-performance supercapacitors.

Keywords: PANi/ERGO thin films, Electrochemical reduction, Charge/discharge, Supercapacitors, Raman spectroscopy.

INTRODUCTION

Supercapacitors can store a hundred times electrical charge compared to standard capacitors and therefore supercapacitors can be a suitable replacement for electrochemical cells for many industrial and commercial applications. The supercapacitors can function at a very low temperature; a circumstance that may impede many sorts of electrochemical cells to function. It is assumed that as the efficiency and energy density of super capacitors increases, the use of advanced energy storage and recovery solutions will become far more widely utilized in the coming years. Although graphene based polyaniline supercapacitors can be a lasting solution in the future, improved technology must be needed to make this reality [1]. Amongst the family of conducting polymers and organic semiconductors, polyaniline (PANi) is a conducting polymer having many alluring processing properties. Due to its rich chemistry, PANi is one of the foremost studied conducting polymers of the last 50 years [2-4]. Polyaniline has three distinct oxidation states with different colours and exhibit acid/base doping response, which makes it particularly attractive. The different charges of the various oxidation states also make PANi more favourable for applications like electrochemical supercapacitors (ESCs). Hetero-atom doped graphene materials or other manufacturing and compromising structural 2D carbides are also the promising uses for micro-supercapacitors [5,6].

Carbon-based material with incorporated or accumulated pseudocapacitive active materials like metal oxides and conducting polymers are used to make composite electrodes [7,8], where carbon based material and implemented pseudo capacitance material provide the capacitor with a particular amount of static double-layer capacitance and a better amount of Faradaic pseudo capacitance. In the recent electrode materials, carbon nanotube is one of the great concerns. As CNTs provide the backbone for an identical allocation of metal oxide or electrically conducting polymers, the electrodes which make from CNTs achieve higher capacitances than either pure carbon or pure metal oxide or polymer based electrodes [9].

A simple, reproducible process to make graphene films from direct electrochemical reduction of GO is delineated. This process accommodates the thickness and size of the graphene film to be pre-determined by thickness and the size of precursor

GO film accumulated on to a gold-coated polyethylene terephthalate electrode. The electrochemically reduced graphene oxide created by this process displayed to be a superb material for energy storage.The specific capacitance noticed for the supercapacitor was 128 F/g, which is on the brink of those of graphene and other carbon materials stated in the literature [10]. A modified Hummers method was used to prepare GO sample and then electrochemical reductions were performed, using applied potentials of -1 to 1.6 V, -1.5 to 0 V and -1 to 1 V. A specific capacitance of 246 F/g was attained at an applied potential of -1 to 1 V for 4000 s [11]. Making graphene sheets, a high voltage of 15 V was applied to disrupt graphite rods electrochemically. As a result, uncontrollable oxidation and structural defects led to be found due to this high potential. Also electrochemical reduction of PANi/GO layer-by-layer (LBL) film is reported with a good specific capacitance at high current density [12]. However, electrochemical reduction of PANi/GO films at different potentials variation with splendid specific capacitance is not reported yet. Polyaniline is conductive polymer, it can help the mobility of electron on the PANi/GO thin film during electrochemical reduction of GO. In this work, polyaniline/graphene oxide thin film was reduced electrochemically with different potential windows, scan rate and number of cycles which was acquired using LBL assembly method. The resultant electrodes displayed various specific capacitances following pre-reduction with different conditions. The optimum conditions were explored for supercapacitor application and a high splendid specific capacitance was attained like the film was reduced with applied potential of -0.87 to -0.5 V. This unique performance of the electrochemically reduced optimized electrode (PANi/ERGO) is the first time reported in best to our knowledge. Also, pure PANi was tested to evaluate the effect on different potential during electrochemical reduction. The influence of the electrochemical reduction was investigated by Raman spectroscopy and X-ray photoelectron spectroscopy for high capacitance performance.

EXPERIMENTAL

The method of graphene oxide (GO) synthesis, formulation of PANi solution and instrumental methods were stated earlier [12-15]. Raman scattering spectra were performed at room temperature on a Raman spectrometer (LabRAM HR, Horiba Jobin Yvon SAS using a 532.8 nm laser). X-ray photoelectron spectroscopy spectra were obtained *via* a Thermo Scientific K5 XPS system (Thermo-Fisher scientific, UK) with a monochromatic AlKα source. All the electrochemical measurements were carried out at ambient conditions in 1 M H_2SO_4 solution using a CHI760C electrochemical work station (CH Instruments Inc., USA), including cyclic voltammograms (CVs), galvanostatic charge-discharge plots (CD) and electrochemical impedance spectroscopy (EIS). The cyclic voltammetric measurements were carried out in an aqueous electrolyte solution (1 M H_2SO_4) at several scan rates using Ivium Stat Technologies system, which includes indium tin oxide (ITO) with an as-prepared PANi/ERGO multilayer film as working electrodes. The Ag/AgCl and Pt wire were employed as the reference and counter electrodes, respectively. The CVs and charge/discharge process were utilized to determine the volumetric capacitance of the electrodes based on 0.125 cm^2 active area and the thickness of the multilayer film composed of 30 Pani/ERGO bilayer, which was determined by optical ellipsometry. No binder or conductive additives were applied. The electrode capacitance was calculated from the CV curves by dividing the current by the voltage scan rate, $C = I/(dV/dt)$ and from charge/discharge curves by using following equation, $C = I \times \Delta t/\Delta V$, where, C = capacitance; I = applied current, t = time and V = potential difference [16,17]. The EIS spectra were fitted with a Randles equivalent circuit model using Z-view software.

RESULTS AND DISCUSSION

Electrochemical reduction of PANi/GO multilayer films: Xia *et al.* [18] explained the quick reduction of hydroxyl and epoxyl on GO sheets by utilizing pulse voltammetries and cyclic voltammograms measurements, at an applied potential of -1.5 to 0 V compared with -1.3 to 0 V. The proper selection of applied potentials in the e-reduction of GO to ERGO films affected significantly a specific capacitance from 128 F/g at constant potential reduction (-1.2 V) to 246 F/g at an applied potential of -1.0 to 1.0 V for 4000 s [19]. Thus, the electrochemical reduction (e-reduction) of GO in PANi/GO multilayer films self-assembled on ITO electrode was assessed in 1 M H_2SO_4 using CVs with different applied potential ranges; -1.3 to -0.87 V, -0.87 to -0.5 V and -1.3 to 1.2 V (*vs.* Ag/AgCl) at a scan rate of 50 mV/s as diplayed in Fig. 1. It was observed that the highest capacitance was achieved for PANi/ERGO films obtained at the potential range of -0.87 to -0.5 V among others, as demonstrated in Fig. 1a. It is noteworthy that the highest capacitance for ERGO films obtained using the potential range of -1 to +1 V [19]. However, it is observed that an electrolyte (1 M H_2SO_4) started to decompose at -0.87 V, while in case of the reduction potential window (-0.87 to -0.5 V), at least 40 cycles were required to complete irreversible reduction (Fig. 1c). Approximately, it was examined the irreversible reduction upto 40 cycles to complete the PANi/ERGO film electrodes. One more observation was recorded that after addition of 1 M H_2SO_4 to the cell, immediate reduction should be completed, otherwise electrochemical reduction would be prohibited even 30 min after no reduction was occured. It is also found that the scan rate has significant influence on the capacitance of the PANi/ERGO multilayer films. The best result of the reduced electrode was achieved at a scan rate of 50 mV/s (Fig. 2). The e-reduction of the PANi/GO multilayer film utilizing the acidic electrolyte supported the formation of the most favourable doping state in the PANi layers, as confirmed by Raman and XPS analysis.

Raman analysis of multilayer films: Raman spectra were applied to characterize the structural change during the electrochemical reduction of GO under various applied potentials. The significant structural changes during the electrochemical process when GO was changed to ERGO were also identified in the Raman spectra (Fig. 3). The Raman spectra of GO includes an observable G peak at 1606 cm^{-1}, resembling the first-order scattering of the E_{2g} mode [12,20]. It has the D peaks at 1190 and 1354 cm^{-1} and other hand, which are at 1181 and 1354

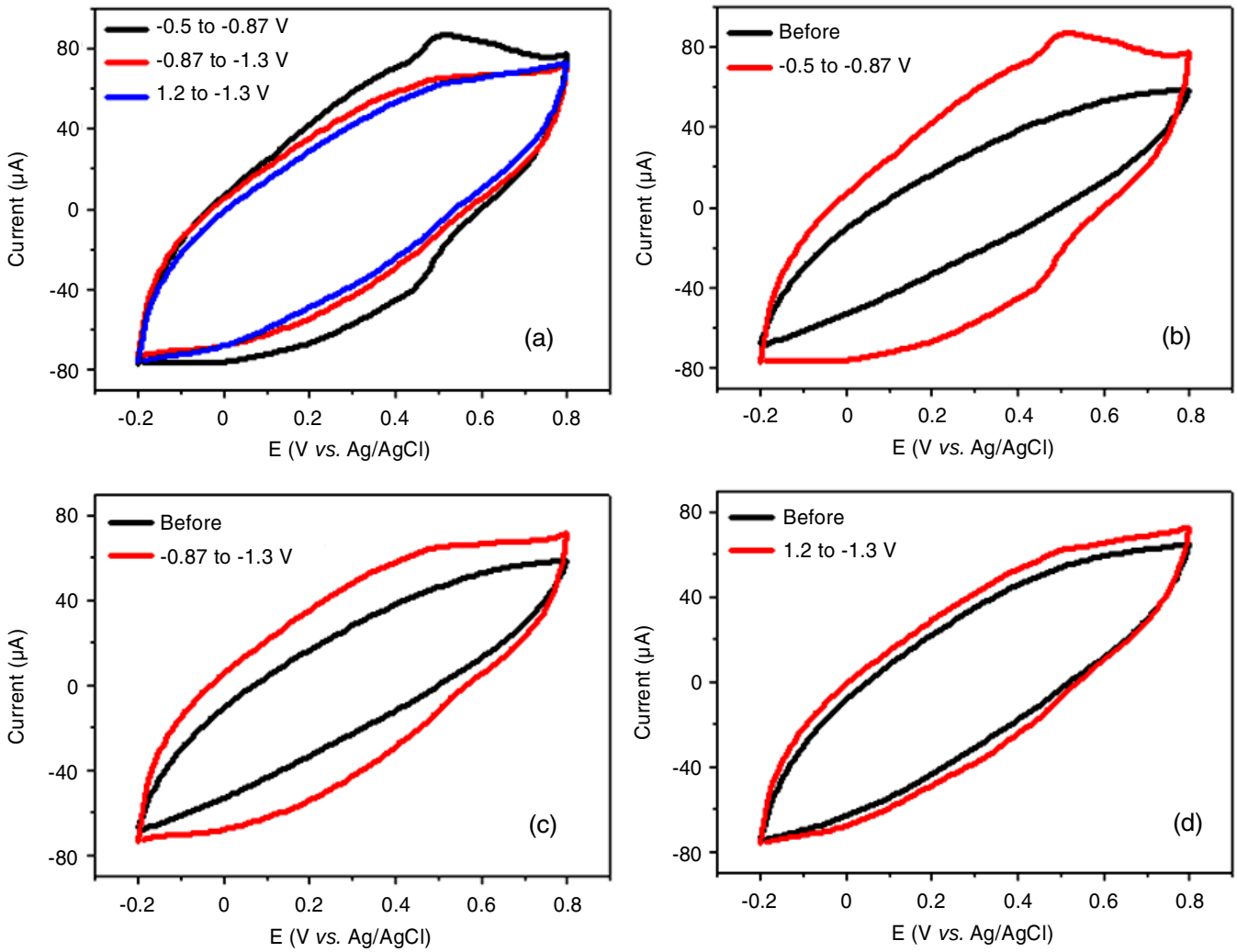

Fig. 1. Cyclic voltammograms obtained during the e-reduction cycles of PANi/GO thin films on ITO electrode, carried out in 1 M $H_2SO_4$with scanning the potential from -1.3 to 1.2 V, -0.87 to -0.5 V and -0.87 to -1.3 V (a), before and after e-reduction at -0.87 to -0.5 V (b), before and after e-reduction at -0.87 to -1.3 V(c) and before and after e-reduction at 1.2 to -1.3 V (d) (*vs.* Ag/AgCl) at a rate of 50 mV/s

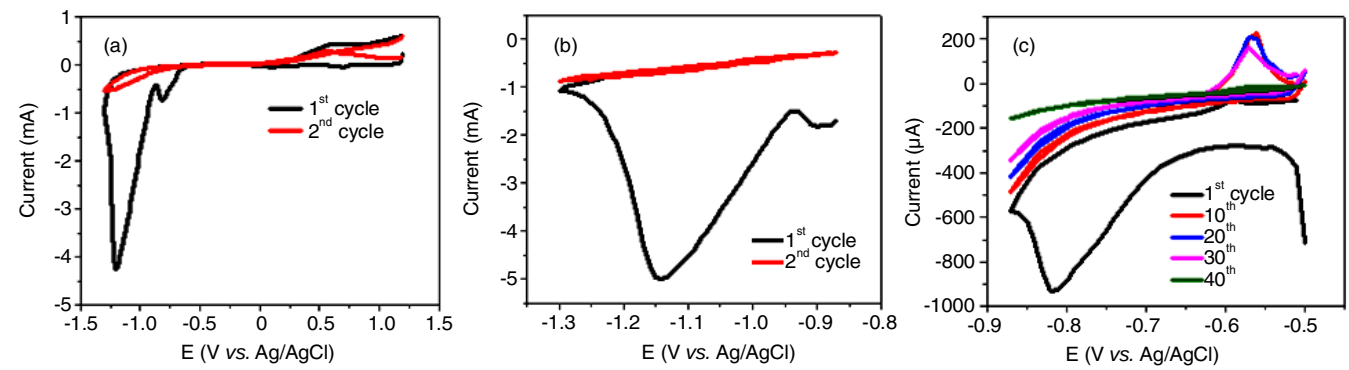

Fig. 2. Cyclic voltammograms obtained during the e-reduction cycles of PANi/GO thin films on ITO electrode, performed in 1 M H_2SO_4 with scanning the potential from -1.3 to 1.2 V (a) -1.3 to -8.7 V (b) -0.87 to -0.5 V (c) (*vs.* Ag/AgCl) at 50 mV/s

cm^{-1} from GO to ERGO showing the structural changes are imposed on the highly disordered and defective morphology of the sheets [21]. The D band at 1190 cm^{-1} is due to the decreased size of in-plane sp^2 domains in the pristine graphite, circumstantially ascribable to comprehensive oxidation. For GO, the D band presenting the disordered carbon, was expanded and overlapped the G band from graphitic carbon, which was caused possibly by comprehensive oxidation. The spectra of the ERGO in the multilayer films contained both the G and D bands (at 1606 and 1354 cm^{-1}, respectively). Following reduction, the D band became acute and easily segregated from the G band. Furthermore, the I_D/I_G ratio was increased from 0.95 for GO

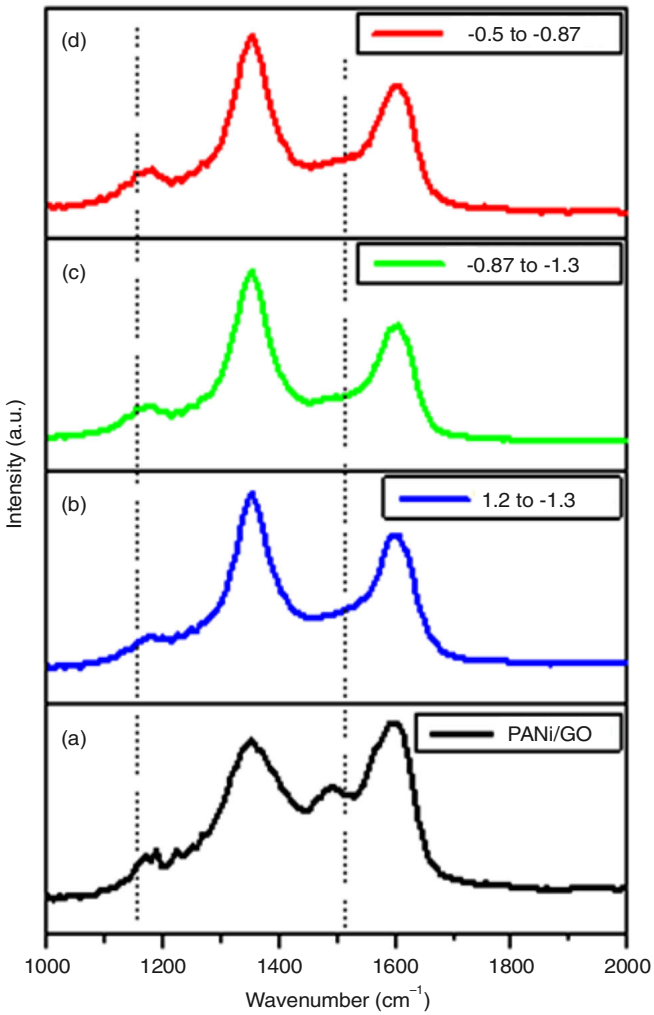

Fig. 3. Raman spectra of PANi/GO thin films on ITO electrode before treatment (a), after treatment of applied potentials -1.3 to 1.2 V (b), -1.3 to -0.87 V (c) and -0.87 to -0.5 V (d), respectively

to 1.22, 1.28 and 1.20 for ERGO at applied potentials of -1.3 to 1.2 V, -1.3 to -0.87 V and -0.87 to -0.5 V, respectively (Table-1). However, the ratio was raised randomly after electrochemical reduction with the applied potentials. This may have been generated by the creation of graphitic domains that were smaller in size. Ferrari *et al.* [22,23] and other reseachers [24-26] indicated an increase in the ratio of I_D/I_G by using hydrazine to reduce GO.

TABLE-1
INTENSITY RATIO OF THE G AND D BANDS IN THE RAMAN SPECTRA

Treatment	Before	-1.3 to -0.87 V	-0.87 to -0.5 V	-1.3 to 1.2 V
I_D/I_G	0.95	1.28	1.20	1.22

Moreover, in reduced form, the changes in the aromatic C–H in-plane and C=N stretching modes of the quinoid moiety in PANi at 1181 and 1354 cm^{-1} were observed. These features were noticed, especially after electrochemical reduction under different applied potentials. These were due to the realignment of the PANi backbones and therefore increased the conjugation, which were directly influenced by the hindered electrostatic interactions among the positively charged PANi and the negatively charged GO, which reduced to neutral ERGO [12].

XPS analysis of multilayer films: XPS spectra were used to characterize the structural change during PANi/GO electrochemical reduction under various applied potentials. The XPS results are shown in Table-2. GO displayed a massively oxygenated carbon in the C 1s XPS result: C-C (284.0 eV), C-OH (285.7 eV) and C-O (286.5 eV) were detected at 26.18, 43.89 and 26.92%, respectively (Fig. 4). The allocation of the residual functional groups in graphene, as acquired by electrochemical reduction, varied according to the applied potential [27]. It revealed the deoxygenation occured during the e-reduction process [17] and indicated the existence of oxygenated functional groups on the GO sheets [28]. It consisted of the highly active surface area into the pores of the functional groups having the intercalation-deintercalation of the mobilations. The best reduction was filed with an applied potential of -1 to 1 V, which is not shown in Table-1. Therein case, as displayed by the results of the C1s XPS spectra, a peak corresponding to O=C-OH was not observed and therefore the ratio corresponding to C-O-C was decreased to 19.2%, while that for C-OH, it had been increased to 19.7%. Table-2 showed the fitting outcomes from C1s spectra of ERGO with applied potential for -1.3 to -0.87 V and -0.87 to -0.5 V and -1.3 to 1.2 V, respectively. The outcomes expressed the number of sp^2 carbon groups was increased with the extension of negative potentials. Comparing with different potential ranges, the reduction level of GO in the case of a given potential of -0.87 to -0.5 V was lower than -1.3 to -0.87 V. All the peaks were consistent to the previous reports [17,27-30]. Still, it had a much bigger specific capacitance, possibly due to the large active area sites to their difference of structure.

TABLE-2
FITTING RESULTS (%) OF THE C 1s XPS SPECTRA BEFORE AND AFTER ELECTROCHEMICAL PRE-REDUCTION OF PANi/GO

Treatment	Amount of oxygen (%)	C-O (288 eV)	C-OH (285 eV)	C-C (284 eV)
Before	27.8	26.92	43.89	26.18
-1.3 to -0.87 V	13.4	12.20	36.92	50.85
-0.87 to -0.5 V	13.5	18.20	32.30	49.48
-1.3 to 1.2 V	15.4	5.36	45.86	48.77

TABLE-3
(a) VOLUMETRIC AND AREAL CAPACITANCE MEASURED BASED ON CYCLIC VOLTAMMOGRAMS AND (b) VOLUMETRIC AND AREAL CAPACITANCE MEASURED BASED ON GALVANOSTATIC CHARGE-DISCHARGE CURVES OF -0.87 TO -0.5V ELECTRODE

(a) Volumetric and areal capacitance (CV)						(b) Volumetric and areal capacitance (CD)					
1 mV/s	3 mV/s	5 mV/s	10 mV/s	20 mV/s	50 mV/s	5 A/cm^3	10 A/cm^3	20 A/cm^3	30 A/cm^3	50 A/cm^3	100 A/cm^3
2619	2168	1855	1509	1250	1046	3748	2583	1903	1588	1269	931
18.38	15.22	13.02	10.59	8.77	7.34	26.31	18.13	13.36	11.15	8.90	6.54

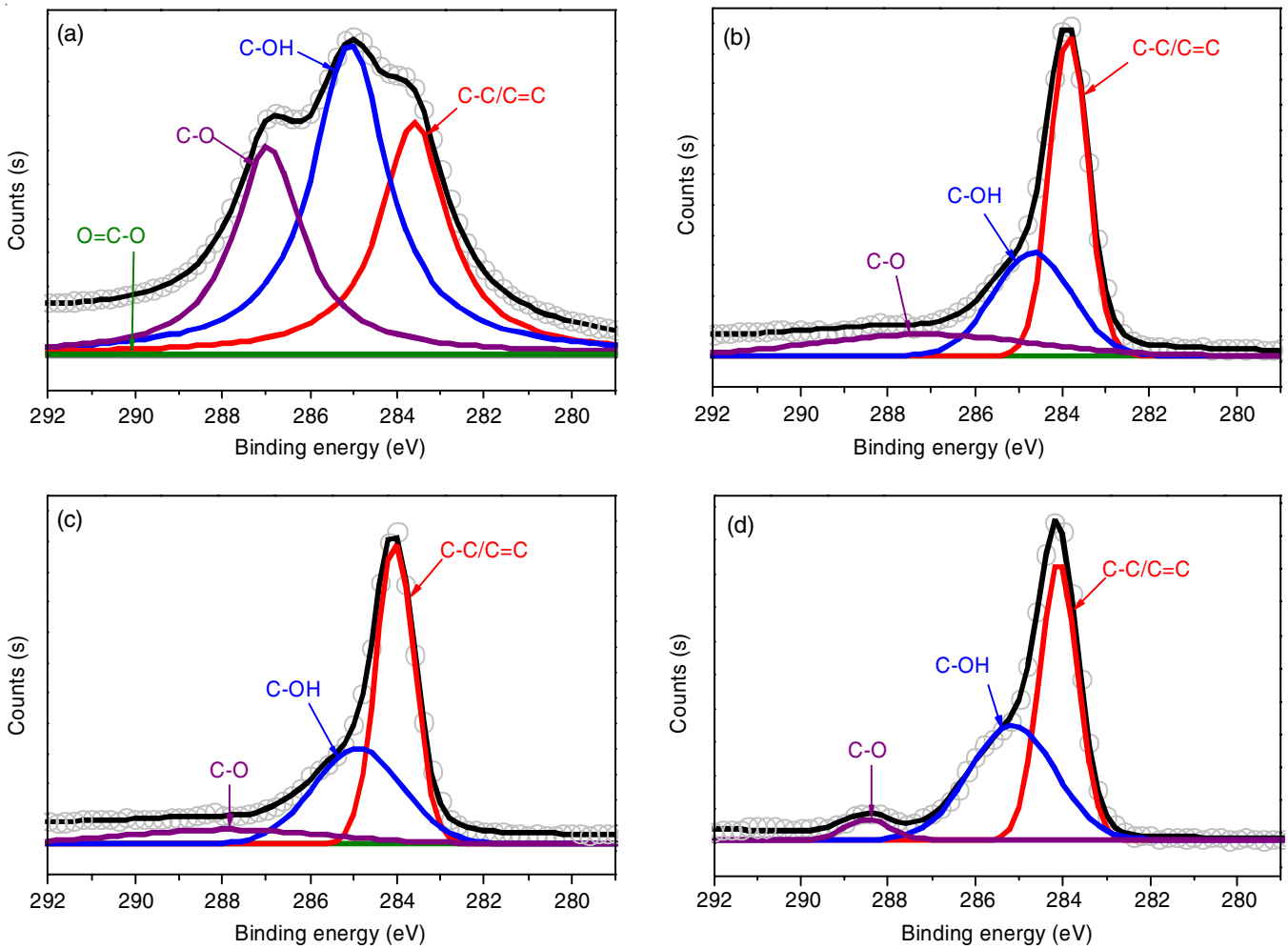

Fig. 4. X-ray photoelectron (XPS) narrow scan spectra of the C1s XPS spectra of PANi/GO before (a) and after electrochemical pre-reduction at -1.3 to -0.87V (b), -0.87 to -0.5V (c) and -1.3 to 1.2V (d) respectively

Supercapacitor performances: For the electrochemical experiments of the prepared electrodes, the distinctive performances were observed by the cyclic voltammetry (CV), galvanostatic charge/discharge (CD) and electrochemical impedance spectroscopy (EIS) measurements in 1 M H_2SO_4 electrolyte solution within a potential range of -0.2 to +0.8 V. The effects of PANi/GO reduction to capacitance were examined under 3 sorts of scanning potential windows: -1.3 to -0.87 V, -0.87 to -0.5 V and -1.3 to 1.2 V, respectively. The PANi/ERGO electrodes utilized as working electrodes were achieved using layer-by-layer assembly method on ITO. Following electrochemical reduction with an applied potential of -0.87 to -0.5 V, the resultant PANi/ERGO electrode showed a good charge discharge process in cyclic voltammetry as the best performer among the mentioned three electrodes. Fig. 5a showed the characteristic CV curves for all the three electrode samples at a scan rate of 100 mV s^{-1} in 1 M H_2SO_4 electrolyte solution within a potential range of -0.2 to +0.8 V indicating the similar shape of CV curves. Table-3 showed the corresponding CV volumetric and areal capacitances. However, the pattern of the CV curves becomes typical of a regular quasi-rectangular shape and resembles the reported data [31-34]. The cyclic voltammogram usually show a pseudo-capacitive behaviour with excellent high-rate competency, effective interlayer charge transfer and the ideal capacitive characteristic of the samples [35,36].

A rectangular-shaped CV (including redox peaks) appeared within the 1 M H_2SO_4 electrolyte, which expressed the PANi/ERGO electrode generating a large amount of pseudo capacitance and a comparatively large amount of double-layer capacitance. Such pseudo capacitance peaks of surface functionalities have also been shown for chemical reduction of PANi/GO film with the HI/H_2O vapour reduction method [12]. Moreover, further work has exhibited that the electrochemical reduction of PANi/GO electrodes was sharply affected by the number of reduction cycles. Fig. 2 showed that 40 cycles are required to complete irreversible reduction of PANi/GO film at potenital of -0.87 to -0.5 V. Likewise, the specific capacitances of PANi/ERGO-based capacitors were found to be maximum at 1493, 2110 and 2619 F cm^{-3} at a scan rate of 1.0 mV s^{-1} for the PANi/GO with applied potentials of -1.3 to 1.2 V and -1.3 to -0.87 V and -0.87 to 0.5 V respectively (Table-4).

A comparison of the CVs and charge/discharge curves indicated the PANi/ERGO electrode obtained by the potential window of -0.2 to 0.8 V showed the regular quasi-rectangular and the near-triangular shapes of the charge/discharge plots (Fig. 5). The CVs in Fig. 5a illustrated that within the three

TABLE-4
VOLUMETRIC CAPACITANCE MEASURED BASED ON CYCLIC VOLTAMMETRY AT SCAN RATE 1 AND 100 mV s^{-1}

Treatment	Specific capacitance (F cm^{-3})	
	1 mV s^{-1}	100 mV s^{-1}
Pre-reduction -0.87 to -0.5 V	2619	874
Pre-reduction -1.3 to -0.87 V	2110	697
Pre-reduction -1.3 to 1.2 V	1493	482

electrodes, the -0.87 to -0.5 V electrode generated the highest rectangular CV curve, including redox peaks, introducing an excellent charge propagation among the electrodes. This outcome proposed a benign capacitance behaviour in addition to an improved electrochemical performance, even given the simple composition of the system, as compared to the nature of commercial cells arrayed with a metal current collector, binders and electroactive additive. The characteristic charge/discharge curves of all electrodes at a current density 3.0 A cm^{-3} are shown in Fig. 5b. Interestingly, the -0.87 to -0.5 V electrode shows much longer discharging period and lowest IR drop as compared to others.

The PANi/ERGO electrode were studied thoroughly over different potential ranges. No significant damage occurred after electrochemical reduction of pure PANi when applied as negative potential. In Fig. 6a, CV curves of the -0.87 to -0.5 V electrode acquired by changing the scan rates remained similar in shape and exhibited no distortions. Furthermore, the -0.87 to -0.5 V electrode revealed a linear relationship observing in the capacitive region with $R^2 = 0.9999$, between the discharge currents and the scan rates (Fig. 6b) indicating a high-power ability for the electrochemical supercapacitors [12]. The rate performance of the electrode was evaluated based on the volumetric capacitances, which acquired from the CV curves over a comprehensive range of scan rate as shown in Fig. 6c and over a discharge range of CD curves (Fig. 6d), which revealed the previous report [12,16,17]. The higher Cs value of -0.87 to -0.5 V compared to two other electrodes can be imposed on the higher electrical conductivity and oxygen vacancies on the higher surface area due to the smaller particle size of the electrode materials.

A representative CV curves for the -0.87 to -0.5 V electrode at scan rate of 1, 5, 10 mV s^{-1} (Fig. 6a) showed the near rectangular shape including redox peaks whereas the corresponding CD curves at current density of 5, 10, 20 A cm^{-3} as shown in Fig. 6e. The electrode demonstrated a specific capacitance of 2619 F cm^{-3} (areal capacitance 18.38 mF cm^{-2}) at a scan rate of 1 mV s^{-1}, which is greater than other values. This is a noticeable progress within the capacitance, compare to supercapacitors based on pure RGO or pure PANi, which also expressed impoverished stability during the charge/discharge cycling. The IR drop of the discharge curve for the -0.87 to -0.5 V electrode was much smaller than that noticed for others, indicating lower interior device resistance. Low interior resistance is significant for energy storing devices; low energy is attenuated by releasing unwanted heat during the charging/discharging processes. The best volumetric capacitance of the -0.87 to -0.5 V electrode introduces one of being best records for capacitance based on carbon materials including conducting polymers.

The electrode rate performance was assessed based on the volumetric capacitances, which attained from the CV curves over the range 1-100 mV/s (Fig. 6c). The highest specific capacitance of the electrode reduced exponentially upon rising the current density and approached to a value of 874 F cm^{-3} at 100 mV s^{-1}. To further exhibit the high capability of the -0.87 to -0.5 V electrode, a Ragone plot of volumetric power density (P_D) *versus* energy density (E_D) was plotted and summarized in Fig. 6f. The galvanostatic charge-discharge (CD) method was examined to analyze the capacitive performance of the electrodes. The CD plots of the -0.87 to -0.5 V electrode at discharge current densities are presented in Fig. 6d. The CD plots of the electrode showed a nearly linear CD profile without any IR drop, as consistent with the CV results (Table-3). In contrast, the Cs value of the electrode was *ca.* 3748 F cm^{-3} (volumetric capacitance) and 26.31 mF cm^{-2} (areal capacitance) at the current density of 5 A cm^{-3}, respectively. This substantial enhancement of Cs value of the electrode could be associated to improve electrical conductivity, which was consistent with

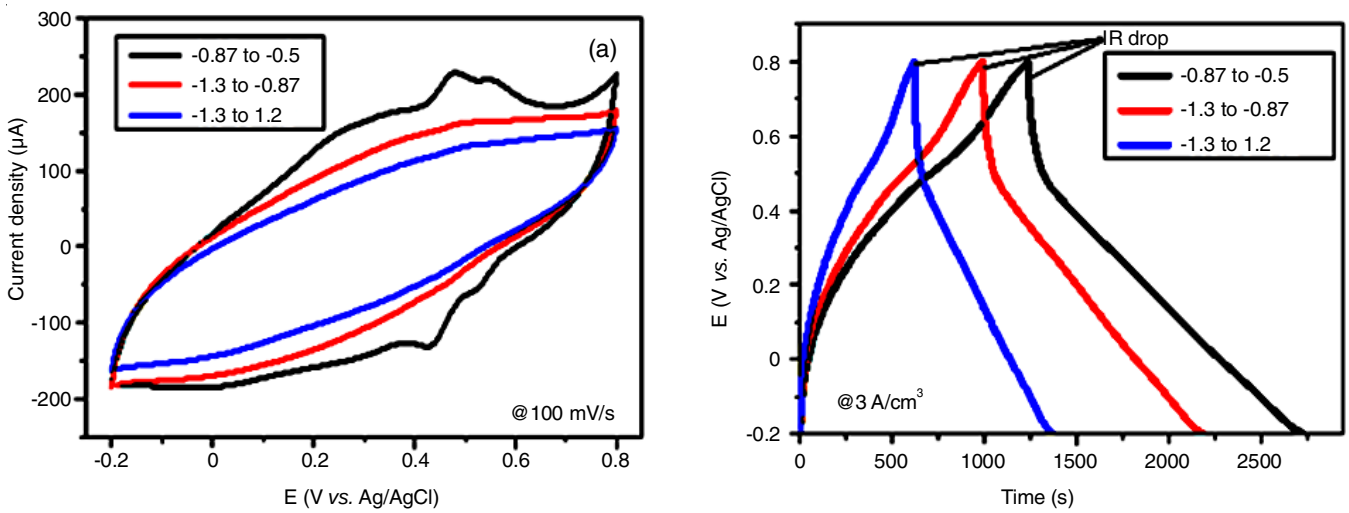

Fig. 5. Comparison of cyclic voltammograms of (a) -0.87 to -0.5V, -1.3 to -0.87V and -1.3 to 1.2V three electrodes at a scan rate of 100 mV/s and (b) Charge/discharge curves of the same in 1 M H_2SO_4, at current density 3 A/cm^3

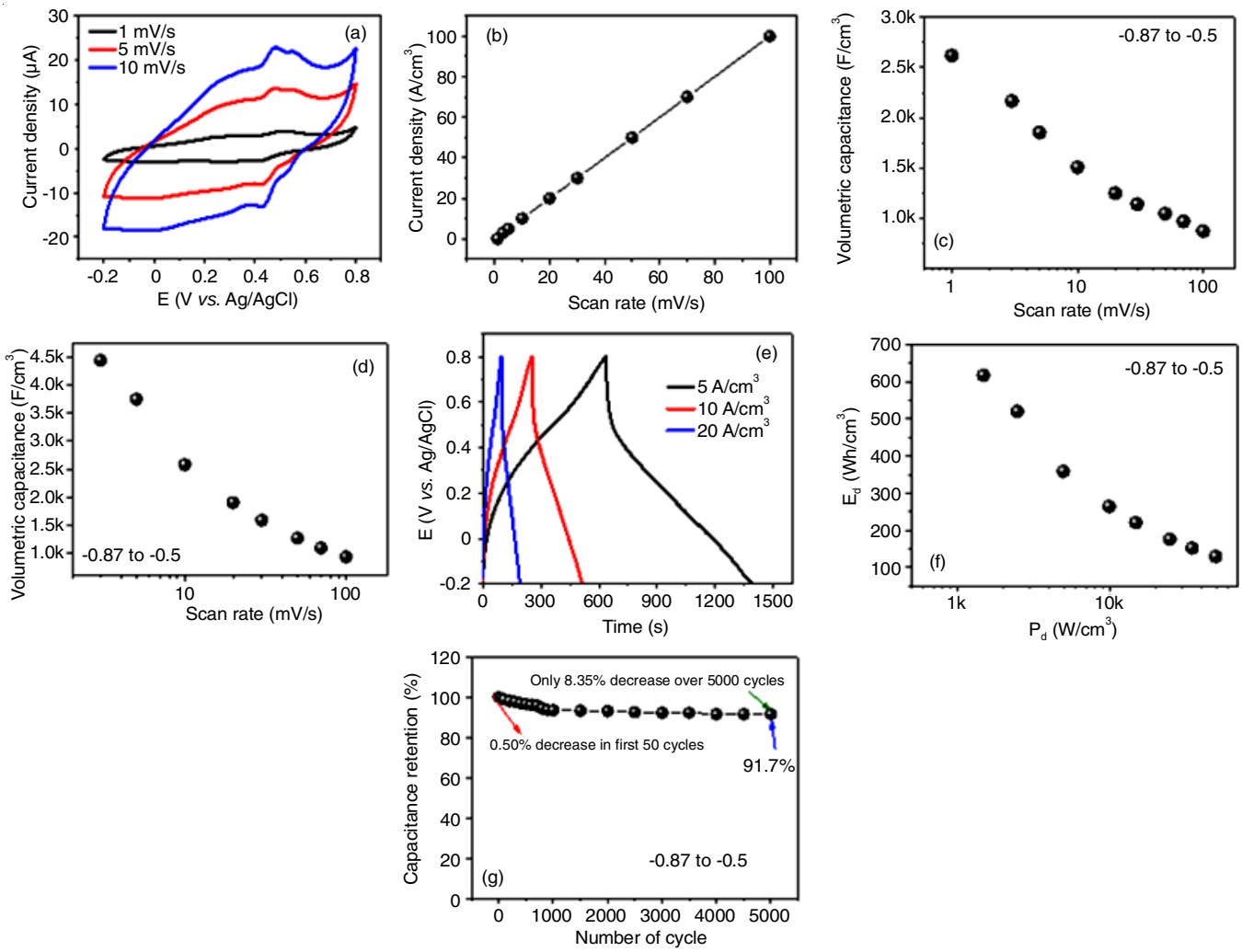

Fig. 6. The -0.87 to -0.5 V PANi/ERGO electrode (a) cyclic voltammograms at 1(black), 5 (red) and 10 mV s^{-1} (blue) scan rates, (b) galvanostatic discharge current density *versus* scan rate, (c) volumetric capacitance as a function of the scan rate obtained from the CV data, (d) volumetric capacitance as a function of the current densities obtained from the charge-discharge data, (e) galvanostatic charge-discharge curves at 5 (black), 10 (red) and 20 (blue) A cm^{-3} current density, (f) Ragone plot of power density *versus* energy density calculated from galvanostatic discharge for all capacitances of -0.87 to -0.5V sample and (g) capacity retention curve over 5000 cycles

the morphological, E_g and XPS analyses. The E_d and P_d of the electrodes were calculated according to the eqns. 1 and 2, respectively [37,38].

$$\text{Energy density } (E_d) = 0.5 \times C_s \times (V_2 - V_1)^2 \times 0.2778 \quad (1)$$

$$\text{Power density } (P_d) = \frac{E_d \times 3600}{\Delta t} \quad (2)$$

The E_d of the -0.87 to -0.5 V, -1.3 to -0.87 V and -1.3 to 1.2 V electrodes were *ca.* 520.7, 419.3 and 295.9 Wh cm^{-3} with the P_d of 2.5 k, 1.9 k and 1.4 k W cm^{-3}, respectively, at a current density of 5 A cm^{-3}. When the P_d increased close to 49.6 k W cm^{-3}, the E_d of the electrode was *ca.* 129.5 Wh cm^{-3} at a current density of 100 A cm^{-3}. The E_d of the -0.87 to -0.5 V electrode is much higher as compared to the other electrode materials (Table-5). This results further suggest that the -0.87 to -0.5 V is the best promising electrode for the commercial development of ESCs with high energy density.

The stability of the electrode materials is immensely significant for the long-term maintenance of supercapacitors. Therefore long-term electrochemical durability of the electrode was evaluated by cyclic CD measurements for 5,000 cycles at 50 A cm^{-3}. Fig. 6g represented the Cs retention (%) of the electrode as a function of the number of CD cycles. Even the electrode displayed a very low Cs loss (*ca.* 0.50) after 50 CD cycles, which could be attributed to the good crystallinity of the material. The highest specific capacitance of the electrode diminished only by 8% even after 5000 charge/discharge cycles indicating a high durability as shown in Fig. 6g. Nevertheless, the little reduction of the C_s after CD cycling is probably owing to the changes in the volume of the electrode induced by the repeated redox reactions while cycling.

The cycling stability of the electrodes was further analyzed by EIS spectra. Fig. 7a showed the comparison EIS spectra of all the electrodes and Fig. 7b-d showed the high frequency region of the same three electrodes, respectively. Table-6 summarized the corresponding EIS fitted parameters of all the electrodes. All the EIS spectra represented a well-defined semicircle in the high-frequency region due to the charge transfer resistance

TABLE-5
VARIOUS ELECTROCHEMICAL PARAMETERS OF THE PANi/ERGO ELECTRODES

Parameters/treatment		Pre-reduction -0.87 to -0.5 V	Pre-reduction -1.3 to -0.87 V	Pre-reduction -1.3 to 1.2V
Areal capacitance (mF/cm^2) (from CV curves @ 1 mV/s scan rate)		18.38	–	–
Areal capacitance (mF/cm^2) (from CD curves @ 5 A/cm^3 current density)		26.31	–	–
Volumetric capacitance (F/cm^3) (from CV curves @ 1 and 100 mV/s scan rate)		2619/874	2110/697	1493/482
Volumetric capacitance (F/cm^3) (from CD curves @ 5 A/cm^3 current density)		3748	3019	2130
Energy density ($Wh\ cm^{-3}$)	At a current density of 5 A/cm^3	520.69	419.33	295.85
	At a current density of 50 A/cm^3	176.27	–	–
	At a current density of 100 A/cm^3	129.45	–	–
Power density ($W\ cm^{-3}$)	At a current density of 5 A/cm^3	2.5k	1.9k	1.4k
	At a current density of 50 A/cm^3	24.8k	–	–
	At a current density of 100 A/cm^3	49.6k	–	–

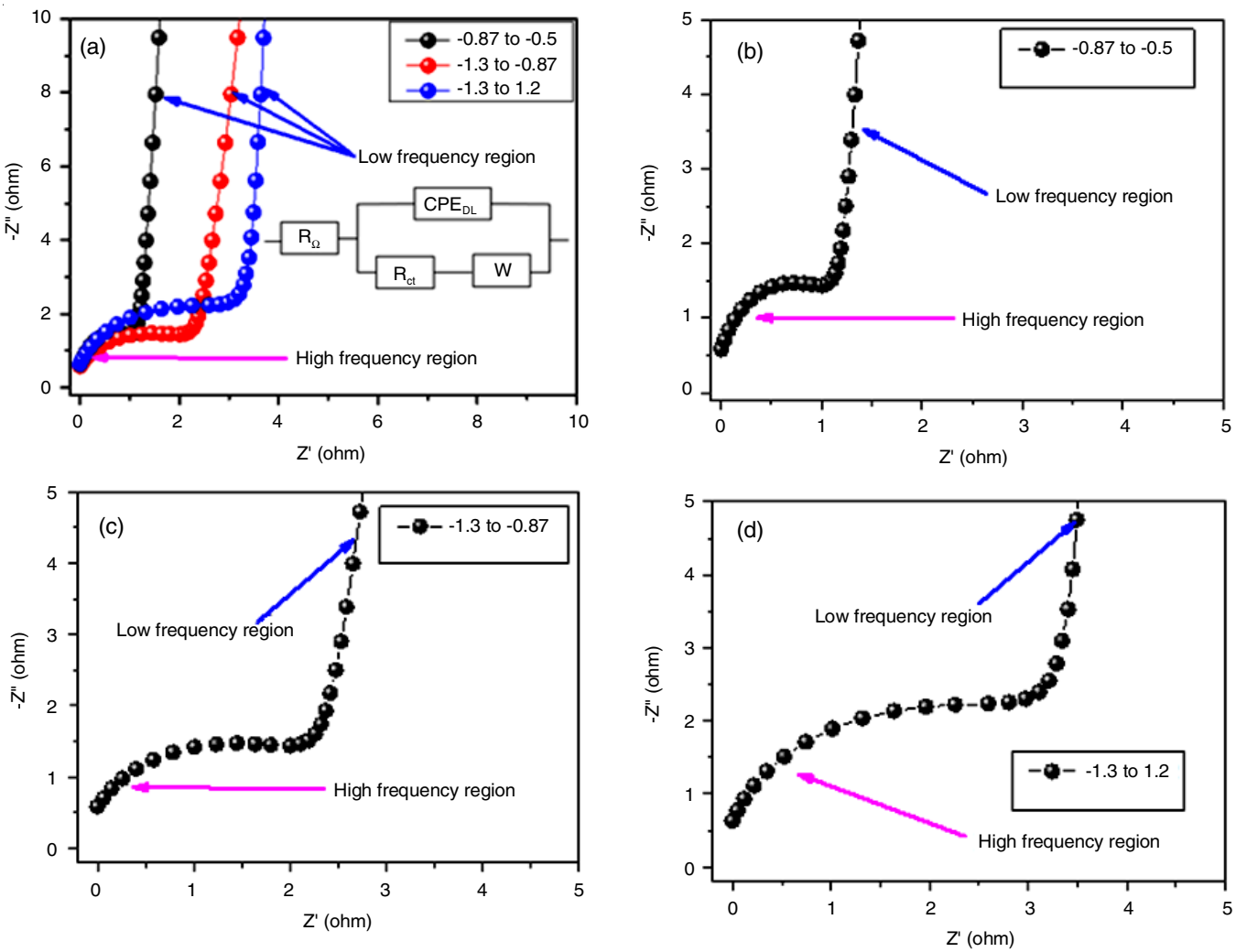

Fig. 7. Nyquist plots of all the samples (a). Same for the high frequency region for -0.87 to -0.5V (b), -1.3 to -0.87V (c), -1.3 to 1.2 V samples (d). Inset of (a) shows the Randles equivalent circuit model to fit the EIS spectra, where CPE_{DL} is the double layer capacitance

(R_{ct}) at the electrode/electrolyte interface and a straight line of Warburg diffusion (Z_w) in the low-frequency region [12,31, 37,38]. A very low solution resistance (R_s) of all the electrodes demonstrate the good adhesion of the materials. Before CD cycling, the R_{ct} of the -0.87 to -0.5 V (a), -1.3 to -0.87 V (b), -1.3 to 1.2 V (c) electrodes was *ca.* 0.502, 1.18 and 1.22 Ω, respectively, while these values were *ca.* 1.8, 16.7 and 30.9 Ω, respectively. And the consistent CPE_{DL} values of the electrodes were *ca.* 9.74, 17.25 and 23.65 μF respectively. Fig. 8a showed the EIS spectra before and after CD cycling of the -0.87 to -0.5 V electrode sample, Fig. 8a (inset) showed the EIS fitted parameters and Fig. 8b showed the high frequency region of the same before and after CD cycling. Before and after CD cycling, the R_s values of the electrode was *ca.* 0.50 and 0.58 Ω, while these values of R_{ct} were *ca.* 1.8 and 2.1 Ω, respectively. These small variations of R_s and R_{ct} before and after CD cycling

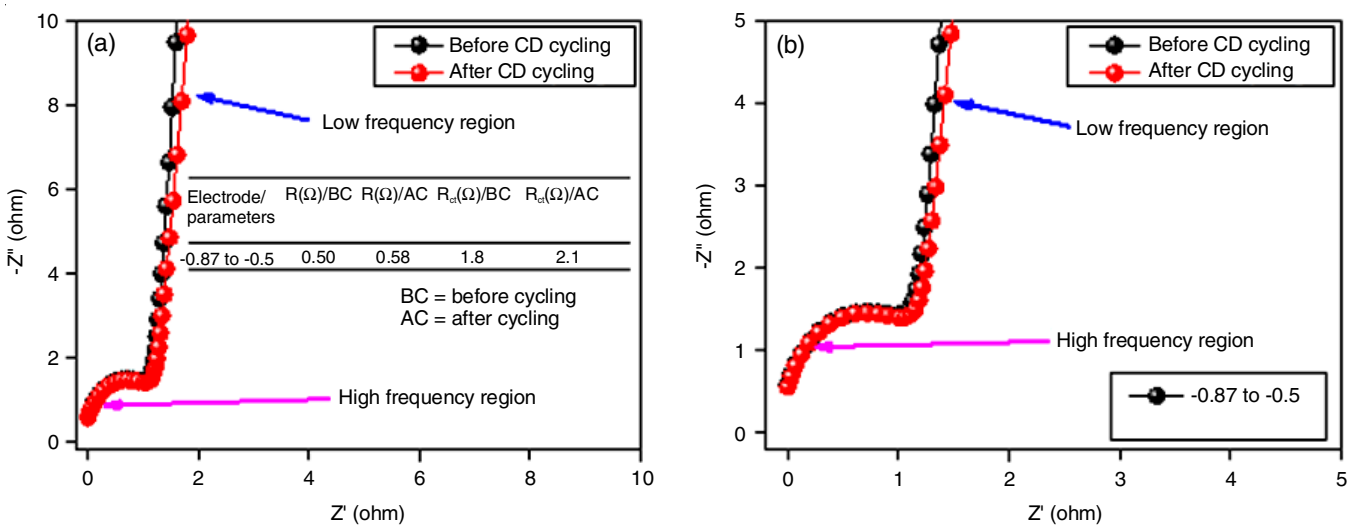

Fig. 8. Nyquist plots of (a) -0.87 to -0.5 V electrode samples before and after CD cycling measured under open-circuit condition. (b) Same for the high frequency region. Inset table (a) summarizes the EIS parameters of the electrodes before and after CD cycling

TABLE-6
FITTED DATA OF EIS SPECTRA OF
ALL THE SAMPLE ELECTRODES

Electrode/parameters	R_s (Ω)	R_{ct} (Ω)	CPE_{DL} (μF)
-0.87 to -0.5	0.502	1.8	9.74
-1.3 to -0.87	1.180	16.7	17.25
-1.3 to 1.2	1.220	30.9	23.65

allocated the high long-term durability of the excellent electrode materials, which are promising for the development of highly stable electrochemical supercapacitors.

Conclusion

In summary, polyaniline/graphene oxide (PANi/GO) thin film microelectrodes were prepared electrochemically reduction with applied different potential windows, scan rate and number of cycles, which was acquired using layer-by-layer (LBL) assembly method. The resultant electrodes displayed various specific capacitances following pre-reduction with different conditions. The optimum conditions were explored for supercapacitor application and an elevated specific capacitance 2619 F cm^{-3} (areal capacitance 18.38 mF cm^{-2}) at 1 mV s^{-1} obtaining the film reduced with an applied potential of -0.87 to -0.5 V. This led to decrease the optical band gap and the charge-transfer resistance (R_{ct}) of -0.87 to -0.5 V at the electrode/electrolyte interface compared to the other two conditions.The influence of the electrochemical reduction was investigated by Raman and X-ray photoelectron spectroscopies for the capacitance performance. The electrode exhibited an enormous electrochemical stability with the Cs net loss of only *ca.* 8% over 5000 CD cycles. This research could pioneer the new possibilities for the development of the effects of the electrochemical reduction to the composite materials for high-performance supercapacitors.

CONFLICT OF INTEREST

The authors declare that there is no conflict of interests regarding the publication of this article.

REFERENCES

1. H. Wang, Q. Hao, X. Yang, L. Lu and X. Wang, *Nanoscale*, **2**, 2164 (2010); https://doi.org/10.1039/c0nr00224k
2. X. Rui, H. Tan and Q. Yan, *Nanoscale*, **6**, 9889 (2014); https://doi.org/10.1039/C4NR03057E
3. K.D. Fong, T. Wang and S.K. Smoukov, *Sustainable Energy Fuels*, **1**, 1857 (2017); https://doi.org/10.1039/C7SE00339K
4. S.A. Ansari, N.A. Khan, Z. Hasan, A.A. Shaikh, F.K. Ferdousi, H.R. Barai, N.S. Lopa and M.M. Rahman, *Sustainable Energy Fuels*, **4**, 2480 (2020); https://doi.org/10.1039/D0SE00049C
5. Z. Peng, R. Ye, J.A. Mann, D. Zakhidov, Y. Li, P.R. Smalley, J. Lin and J.M. Tour, *ACS Nano*, **9**, 5868 (2015); https://doi.org/10.1021/acsnano.5b00436
6. C. Zhang, L. McKeon, M.P. Kremer, S.-H. Park, O. Ronan, A. Seral-Ascaso, S. Barwich, C.Ó. Coileáin, N. McEvoy, H.C. Nerl, B. Anasori, J.N. Coleman, Y. Gogotsi and V. Nicolosi, *Nat. Commun.*, **10**, 1795 (2019); https://doi.org/10.1038/s41467-019-09398-1
7. J.H. Chen, W.Z. Li, D.Z. Wang, S.X. Yang, J.G. Wen and Z.F. Ren, *Carbon*, **40**, 1193 (2002); https://doi.org/10.1016/S0008-6223(01)00266-4
8. C. Li, D. Wang, T. Liang, X. Wang and L. Ji, *Mater. Lett.*, **58**, 3774 (2004); https://doi.org/10.1016/j.matlet.2004.07.027
9. C. Peng, S. Zhang, D. Jewell and G.Z. Chen, *Prog. Nat. Sci.*, **18**, 777 (2008); https://doi.org/10.1016/j.pnsc.2008.03.002
10. X.Y. Peng, X.X. Liu, D. Diamond and K.T. Lau, *Carbon*, **49**, 3488 (2011); https://doi.org/10.1016/j.carbon.2011.04.047
11. W. Lu, J.B. Baek and L. Dai, Carbon Nanomaterials for Advanced Energy Systems: Advances in Materials Synthesis and Device Applications, John Wiley & Sons Inc., United States of America, p. 323 (2015).
12. A.K. Sarker and J.D. Hong, *Langmuir*, **28**, 12637 (2012); https://doi.org/10.1021/la3021589
13. G. Decher and J.D. Hong, *Makromol. Chem. Macromol. Symp.*, **46**, 321 (1991); https://doi.org/10.1002/masy.19910460145
14. G. Decher and J.D. Hong, *Ber. Bunsenges. Phys. Chem*, **95**, 1430 (1991); https://doi.org/10.1002/bbpc.19910951122
15. G. Decher, J.D. Hong and J. Schmitt, *Thin Solid Films*, **210-211**, 831 (1992); https://doi.org/10.1016/0040-6090(92)90417-A
16. A.K. Sarker and J.D. Hong, *Colloids Surf. A Physicochem. Eng. Asp.*, **436**, 967 (2013); https://doi.org/10.1016/j.colsurfa.2013.08.043

17. A.K. Sarker and J.D. Hong, *Bull. Korean Chem. Soc.*, **35**, 1799 (2014); https://doi.org/10.5012/bkcs.2014.35.6.1799
18. H. Guo, X. Wang, Q. Qian, F. Wang and X.A. Xia, *ACS Nano*, **3**, 2653 (2009); https://doi.org/10.1021/nn900227d
19. H. Yu, J. He, L. Sun, S. Tanaka and B. Fugetsu, *Carbon*, **51**, 94 (2013); https://doi.org/10.1016/j.carbon.2012.08.016
20. F. Tuinstra and J.L. Koenig, *J. Chem. Phys.*, **53**, 1126 (1970); https://doi.org/10.1063/1.1674108
21. A. Kaniyoor and S. Ramaprabhu, *AIP Adv.*, **2**, 032183 (2012); https://doi.org/10.1063/1.4756995
22. A.C. Ferrari, *Solid State Commun.*, **143**, 47 (2007); https://doi.org/10.1016/j.ssc.2007.03.052
23. A.C. Ferrari, J.C. Meyer, V. Scardaci, C. Casiraghi, M. Lazzeri, F. Mauri, S. Piscanec, D. Jiang, K.S. Novoselov, S. Roth and A.K. Geim, *Phys. Rev. Lett.*, **97**, 187401 (2006); https://doi.org/10.1103/PhysRevLett.97.187401
24. S. Stankovich, D.A. Dikin, R.D. Piner, K.A. Kohlhaas, A. Kleinhammes, Y. Jia, Y. Wu, S.B.T. Nguyen and R.S. Ruoff, *Carbon*, **45**, 1558 (2007); https://doi.org/10.1016/j.carbon.2007.02.034
25. A. Das, B. Chakraborty and A.K. Sood, *Bull. Mater. Sci.*, **31**, 579 (2008); https://doi.org/10.1007/s12034-008-0090-5
26. L.G. Cancado, K. Takai, T. Enoki, M. Endo, Y.A. Kim, H. Mizusaki, N.L. Speziali, A. Jorio and M.A. Pimenta, *Carbon*, **46**, 272 (2008); https://doi.org/10.1016/j.carbon.2007.11.015
27. D.X. Yang, A. Velamakanni, G. Bozoklu, S.J. Park, M. Stoller, R.D. Piner, S. Stankovich, I.H. Jung, D.A. Field, C.A. Ventrice Jr. and R.S. Ruoff, *Carbon*, **47**, 145 (2009); https://doi.org/10.1016/j.carbon.2008.09.045
28. C. Mattevi, G. Eda, S. Agnoli, S. Miller, K.A. Mkhoyan, O. Celik, D. Mastrogiovanni, G. Granozzi, E. Garfunkel and M. Chhowalla, *Adv. Funct. Mater.*, **19**, 2577 (2009); https://doi.org/10.1002/adfm.200900166
29. B. Palys, Handbook of Graphene, In: Biosensors and Advanced Sensors. Wiley-Scrivener, vol. 6, p. 613 (2019).
30. M.A. Raj and S.A. John, *J. Phys. Chem. C*, **117**, 4326 (2013); https://doi.org/10.1021/jp400066z
31. H.R. Barai, A.N. Banerjee, N. Hamnabard and S.W. Joo, *RSC Adv.*, **6**, 78887 (2016); https://doi.org/10.1039/C6RA18811G
32. X. Su, X. Yang, L. Yu, G. Cheng, H. Zhang, T. Lin and F.-H. Zhao, *CrystEngComm*, **17**, 5970 (2015); https://doi.org/10.1039/C5CE00707K
33. C. Wan, L. Yuan and H. Shen, *Int. J. Electrochem. Sci.*, **9**, 4024 (2014).
34. S. Devaraj and N. Munichandraiah, *J. Electrochem. Soc.*, **154**, 80 (2007); https://doi.org/10.1149/1.2404775
35. H. Chen, X. Dong, J. Shi, J. Zhao, Z. Hua, J. Gao, M. Ruan and D. Yan, *J. Mater. Chem.*, **17**, 855 (2007); https://doi.org/10.1039/b615972a
36. T. Nathan, M. Cloke and S.R.S. Prabaharan, *J. Nanomater.*, **2008**, 948183 (2009); https://doi.org/10.1155/2008/948183
37. H.R. Barai, M.M. Rahman, M. Roy, P. Barai and S.W. Joo, *Mater. Sci. Semicond. Process.*, **90**, 245 (2019); https://doi.org/10.1016/j.mssp.2018.10.031
38. H.R. Barai, N.S. Lopa, P. Barai, M.M. Rahman, A.K. Sarker and S.W. Joo, *J. Mater. Sci. Mater. Electron.*, **30**, 21269 (2019); https://doi.org/10.1007/s10854-019-02500-9